physics

MDPI

Review

A Brief Review of Some Recent Precision Casimir Force Measurements

Madhav Dhital and Umar Mohideen *

Department of Physics & Astronomy, University of California, Riverside, CA 92521, USA
* Correspondence: umar.mohideen@ucr.edu

Abstract: Here, we review recent advances in precision Casimir force measurements with both non-magnetic and magnetic materials. In addition, the measurement of the geometric dependence of the Casimir force, both lateral and normal, using uniformly corrugated surfaces is briefly presented. Finally, the measurement of the thermal Casimir force in graphene is discussed.

Keywords: precision Casimir force measurements; geometric dependence of Casimir force; normal Casimir force measurements; lateral Casimir force measurements

1. Introduction

Precision measurements of the Casimir force have been ongoing since they were first published, more than two decades ago [1,2]. The rapid progress in precision measurements between metallic test bodies over this period [3–6] has revealed a puzzling problem through disagreement between experiment and theory. In many experiments performed by different groups, it was found that the predictions of the Lifshitz theory came into conflict with the measurement data if the much-studied relaxation properties of conduction electrons at low frequencies were taken into account in computations (detailed in monograph [7]) and reviews [8,9]. In this paper, we briefly review some of the experimental advances in the University of California(UC)-Riverside group since the publication of the previous reviews [7,10]. In Section 2, we recap the results from the recent precision measurement of the Casimir force between smoother Au-coated surfaces of a sphere and plate for much larger separations from 250 nm to 1300 nm in an ultra-high vacuum, using a more force-sensitive cantilever in the custom-built dynamic atomic force microscope (AFM)-based setup. Here, both ultraviolet (UV) light and Ar-ion cleaning of the Au surfaces were carried out to remove ambiguities of electrostatic patches. In Section 3, we briefly consider experiments on the geometric dependence of the Casimir force using sinusoidal corrugated surfaces. Here, measurements of the lateral Casimir force as well as the normal Casimir force between the two uniformly corrugated surfaces are reviewed. In Section 4, earlier experiments on the role of magnetic fluctuations are reviewed. These experiments, in addition to demonstrating the effect of magnetic permeability, were also able to rule out any prominent role for electrostatic patches as an explanation for the disagreement between experiment and theory. Finally, in Section 5, we review our recent experiment measuring the Casimir force from graphene. Graphene provides many advantages towards understanding the disagreement between precision measurements of the Casimir force and the Lifshitz theory. The reason is that the response of graphene to electromagnetic fluctuations can be deduced from the first principles of quantum electrodynamics, thus eliminating the key uncertainty of the material properties in theoretical calculations of the Casimir force when metal test bodies are used where tabulated values of the permittivity [11] and its extrapolation to zero frequency are needed. Key details in all the experiments mentioned above are (i) independent measurement of the residual electrostatic force between the interacting surfaces; (ii) keeping the contribution of this residual electrostatic force either negligible or small compared with the Casimir force, by using clean experimental surfaces in an ultra-high vacuum chamber; and

check for updates

Citation: Dhital, M.; Mohideen, U. A Brief Review of Some Recent Precision Casimir Force Measurements. *Physics* **2024**, *6*, 891–904. https://doi.org/10.3390/physics6020055

Received: 30 November 2023
Revised: 13 February 2024
Accepted: 22 March 2024
Published: 13 June 2024

(iii) using only surfaces where the residual electrostatic force is independent of distance, allowing its definitive subtraction. In the precision Casimir force measurements with normal metals such as Au, the disagreement between the experimental measurement and the Lifshitz theory, using tabulated values of the permittivity and its extrapolation including the dissipation of the free conduction electrons, remains an unresolved puzzle to date. Note that in Refs. [12,13], an agreement was obtained only by subtracting a hypothetical electrostatic force between a centimeter-size spherical lens and a plate that was ten times larger than the Casimir force. The measurements reviewed below, acquired using magnetic metal surfaces [14,15] and difference force measurements using over layers [16], reconfirm this conclusion to high precision.

2. Recent Precision Casimir Force Measurements to 1.3 μm

The most recent direct precision measurements of the gradient of the Casimir force between an Au-coated surface of a sphere and a plate for separations to 1.3 μm were reported in Refs. [17–20]. A large sphere and plate, rather than two plates, were used to avoid problems with keeping two plates parallel. The schematic of the experiment is shown in Figure 1a. A custom-built ultra-high vacuum atomic force microscope cantilever technique was used to measure the Casimir force between an Au-coated sphere and plate. The resonance frequency shift of this microcantilever is related to the sphere-plate force gradient, as:

$$\Delta f = -\frac{f_0}{2k}\left(\frac{\partial F_{\mathrm{el}}}{\partial z} + \frac{\partial F_{\mathrm{Cas}}}{\partial z}\right), \tag{1}$$

where Δf is the frequency shift, f_0 is the cantilever resonant frequency when no force is applied, k is the cantilever spring constant, F_{el} and F_{Cas} are electrostatic force and Casimir force, respectively. The electrostatic force F_{el} is used for calibration. The following improvements over our previous measurements were achieved [17–20]:

i. Force measurement sensitivity improved by a factor of 10.
ii. An in situ Ar ion beam and UV cleaning procedure for the interacting surfaces were introduced, eliminating the effects of ambiguous electrostatic forces and achieving ultra-high vacuum.
iii. The surface roughness of the plate was reduced by a factor of 2 to 1.08 nm through the use of polished Si wafer substrates and e-beam Au coating, which eliminated uncertainties in separation distance (reduced to a smaller than 10^{-4} effect).
iv. Measurements were made to larger separation distances from 250 to 1300 nm (factor of 2 larger than previously).

The gradient of the Casimir force was measured between the Au-coated hollow glass sphere of $R = 43.446 \pm 0.042$ μm radius and the Au-coated silicon plate. The hollow glass spheres were made from liquid phase and had negligible asphericity with the difference along two perpendicular axes being less than or equal to 0.1%. The spring constant k of this cantilever was reduced by decreasing its thickness through etching with 60% KOH (potassium hydroxide) solution. The electron micrograph of the Au-coated hollow glass spheres attached to the cantilever end is shown in Figure 1b. The use of polished silicon wafer as the base plate instead of sapphire or fused silica plates used previously [6] and an e-beam evaporator for making the Au coatings instead of a thermal evaporator allowed a decrease in the surface roughness by up to a factor of 2. The root-mean square (rms) roughness on the sphere and the plate was 1.13 nm and 1.08 nm, respectively (compared with 2.0 nm and 1.8 nm, respectively, in Ref. [6]). The Au-coated plate was mounted on a piezoelectric tube which helped to precisely control its position, see Figure 1a. The precise plate position was measured with the 520 nm interferometer shown in Figure 1a. The cantilever oscillation was monitored with a 1550 nm laser optical interferometer. The finesse of the cavity was maximized by Au coating the cantilever top end. Care needed to be taken, as Au coating of the cantilever would reduce the oscillator quality factor, Q.

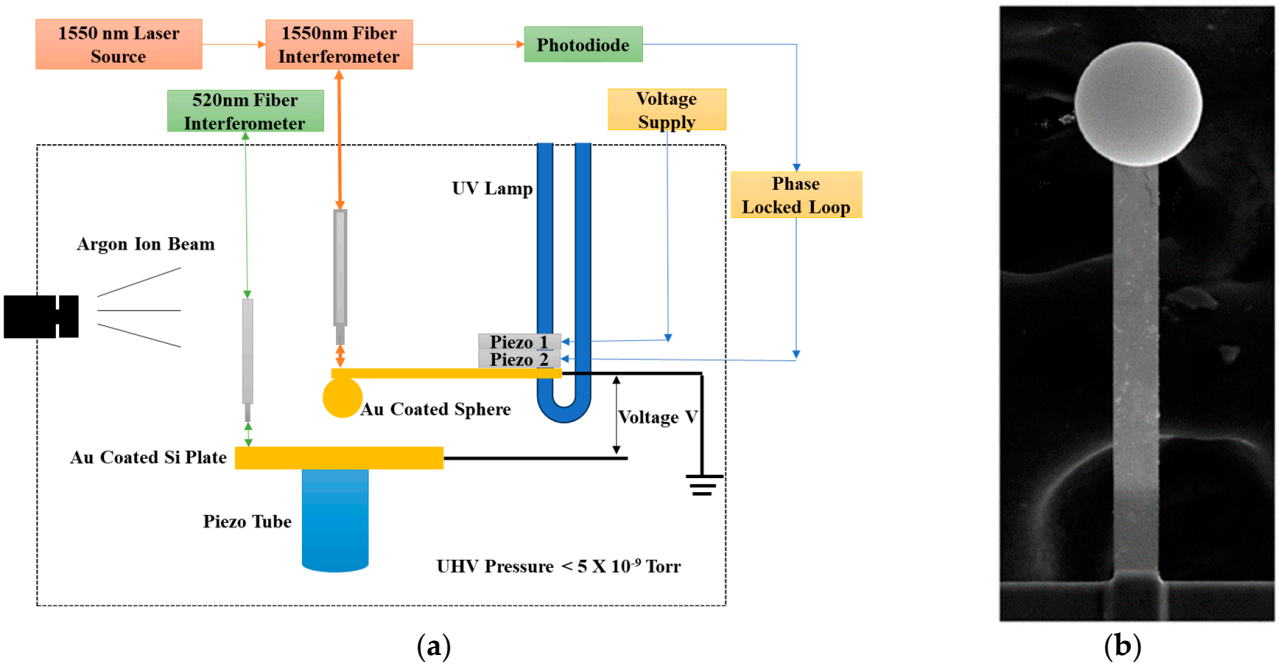

Figure 1. (**a**) Schematic of the experimental setup. "UV" stands for "ultraviolet" and "UHV" stands for "ultra-high vacuum". (**b**) SEM (scanning electron microscope) micrograph of a microcantilever with attached Au-coated sphere.

Removing Ambiguity from Electrostatic Patches

A major improvement over all previous experiments is the in situ UV followed by Ar-ion cleaning of the test bodies and surfaces inside the vacuum chamber. The in situ cleaning of interacting surfaces in Casimir force measurements is critical for the removal of any surface contaminants that lead to background electrostatic forces. In particular, the contaminants lead to inhomogeneous work functions of the Au surface, resulting in patch potentials [21–24]. Such patch potentials result in electrostatic forces having a distance dependence (electric multipole effects), complicating their subtraction and leading to ambiguity in precision measurements of the Casimir force. Traditional vacuum cleaning by baking to high temperatures is not suitable, as the interferometer alignment is destroyed by thermal stress. In Figure 2, the sphere–plate residual potential is shown as a function of separation distance before and after UV plus Ar-ion-beam cleaning. In Ar-ion cleaning, the ions are focused on the interacting sphere–plate surfaces, as shown in Figure 1a, and the adsorbed contaminants on the experimental chamber walls are not completely removed. Thus, over time, the desorption of contaminants from the chamber walls leads to the redeposition of some of the contaminant molecules on the Au surfaces of the test samples, resulting in an increase in residual electric potential difference. First, applying UV light leads to desorption of surface contaminants from the entire chamber, either through direct ionization or reaction with generated ozone, which is then pumped out. As a result of the UV light followed by Ar-ion-beam cleaning, the residual potential difference between sphere and plate, as shown in Figure 2, was lowered by an order of magnitude, leading to the near elimination of electrostatic forces, as discussed in the literature [18,19]. Its value is also independent of sphere–plate separation distance, pointing to the absence of electric multipole effects from any patch effects. In addition, the residual potential difference between the two surfaces remains near zero for considerably longer, allowing stable Casimir force measurements.

The measurement results [18,19] for the gradient of the Casimir force obtained are shown in Figure 3a,b over the separation range from 250 to 950 for 10 nm cantilever oscillation amplitude.

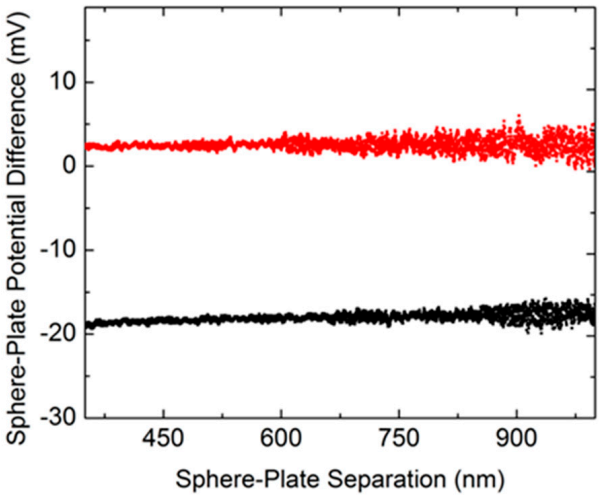

Figure 2. The Au sphere–plate residual potential difference as a function of the separation before (black) and after (red) UV and Ar-ion cleaning [20]. Reproduced under the copyright permission from World Scientific.

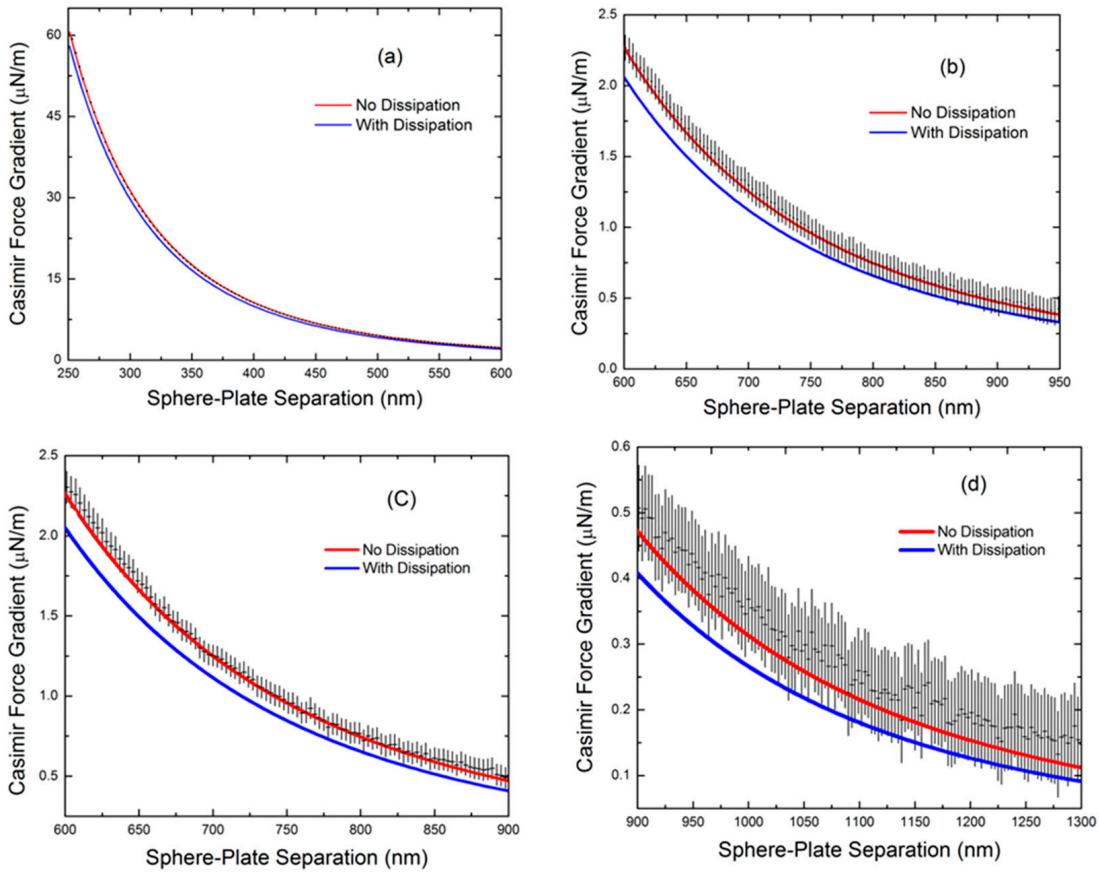

Figure 3. The Casimir force gradient measured as a function of the sphere–plate separation for (**a**,**b**) 10 nm cantilever oscillations and (**c**,**d**) 20 nm cantilever oscillations [18]. The experimental data (error bars) for the force gradient and separation agree with the no-dissipation theory calculations (lines) for zero-point photon-free electron scattering for all separations shown.

Using larger cantilever oscillation amplitudes of 20 nm, the frequency shift measurement can be improved, allowing Casimir force gradient measurements to 1300 nm. The measured gradients are shown as crosses in Figure 3c,d over the separation region from 600 nm to 1.3 μm. The vertical size of the crosses indicates the total error in measuring

the force gradient at the 67% confidence level. The horizontal size is determined by the constant error in measuring the absolute separations Δz = 0.5 nm in Figure 3a,b and 1.1 nm in Figure 3c,d. For ease of visualization, only every third data point is plotted. In the theory calculations, the Au metal response is given by the permittivity $\varepsilon(\omega)$, where the tabulated values in Ref. [11] were used along with the extrapolation to low frequencies made using $\varepsilon(\omega) = \frac{\omega_p^2}{\omega(\omega+i\gamma)}$, where ω_p = 9.0 eV is the plasma frequency and the relaxation frequency is γ = 35 meV [11] for the dissipative Drude model and $\gamma = 0$ for the dissipationless plasma model. The theoretical values represented by the solid blue line were calculated with the tabulated Au permittivity [11] and dissipative Drude extrapolation to zero frequency. The theoretical values represented by the solid red line were calculated with the tabulated Au permittivity [11] and dissipationless plasma extrapolation to zero frequency. As is seen in Figure 3a–d, the theoretical predictions using the dissipationless plasma model are consistent with the measurement data over the entire range from 250 nm to 1.3 μm. The predictions of the Lifshitz theory using the dissipative Drude model are excluded at all separations up to 1.1 μm. Thus, the range of separations where the dissipative Drude model is excluded has been significantly extended.

3. Geometric Dependence of the Casimir Force with Sinusoidally Corrugated Surfaces

3.1. Demonstration of Asymmetry and Nonadditivity in Lateral Casimir Force

Controlling the length scale of the zero-point photon fluctuations using boundary geometry, dielectric properties, and temperature leads to profoundly interesting effects. In particular, uniformly corrugated boundaries are of interest due to the diffraction-type coherent scattering effects of zero-point photons that have been reported in these systems [23,25–34]. The zero-point photon wavelengths that matter are those that correspond to the separation distance. Additional important length scales in the problem are the corrugation period, λ, separation between the corrugations, z, the thermal wavelength $\hbar c/k_B T$, the temperature, T, and the material reflectivity through the plasma wavelength $2\pi c/\omega_p$, where ω_p is the plasma frequency, $\hbar$ is the reduced Planck constant, c denotes the speed of light, and k_B is the Boltzmann constant. The coupling of scales of different lengths and the angle between the two corrugations led to rich behavior, making it a promising probe into these interconnected phenomena [35–40].

Of the above, the most intriguing feature is the nonadditive behavior of the Casimir force and, thus, the complicated dependence on the shape of the boundary surfaces connected with diffraction effects. The nontrivial behavior of the normal Casimir force was experimentally demonstrated in the configuration of a smooth sphere above a sinusoidally corrugated plate [25]. For the case of the additive regime, we reported measurement of the lateral Casimir force between two aligned sinusoidally corrugated surfaces of a sphere and a plate [26]. In the case of the nonadditive regime, the deviation of both the experimental data and the exact theory from the prediction of the proximity force approximation (PFA) was quantified in Refs. [29,30]. PFA approximates curved surfaces as a collection of infinitesimal flat surface elements and the local parallel plate contributions are added [27,28]. Thus, PFA neglects the diffraction effects of the zero-point photons. Compared with our previous lateral force measurement [2,26], this demonstration [29,30] of asymmetry and nonadditivity required many improvements such as a decrease of more than 50% in the grating period along with a 71% increase in the amplitude of the aligned imprinted grating. Here, the experimental chamber with a pressure less than 10 mTorr contained a sinusoidally corrugated Au-coated grating of size 5×5 mm^2 vertically mounted on the piezotube of the AFM. In order to achieve the nonadditive regime, the corrugations had an average period of 574.7 nm, i.e., less than half of that in Refs. [2,26] and an amplitude of 85.4 $\pm$ 0.3 nm, compared with 59 nm in Refs. [2,26]. This flat grating served as the first test body. A 320 μm long V-shaped silicon nitride cantilever for the AFM was specially prepared first by uniformly coating it with 40 nm of Al to improve its thermal and electric conductivity and to prevent deformation due to differential thermal expansion in a vacuum. The lateral Casimir force results from the interaction between two perfectly aligned uniaxially corrugated surfaces of

the same period. With the goal to keep the contact region for the imprinting of the grating and to make the second corrugated surface far away from the silicon nitride cantilever, a 200 ± 4 μm diameter polystyrene sphere was placed at the end of the cantilever, to the bottom of which a freshly cleaved mica sheet of 400 μm length, 200 μm width, and a few micrometers thickness was attached. A second polystyrene sphere was then attached to the bottom free end of the mica sheet. The complete system was uniformly coated with a 10 nm layer of Cr and then with a 50 nm layer of Au in a thermal evaporator. The corrugations of the flat grating were imprinted on the Au-coated sphere using a stepper motor and by applying a voltage to the AFM piezo, as has been described. The lateral Casimir force between the two aligned sinusoidally corrugated Au-coated surfaces was measured for separation distances between 121.1 nm and 175.3 nm, much smaller than the 221–257 nm measured previously. The uncertainty in the measured separation distances was reduced to 4 nm, compared with 32 nm previously [6].

In addition, an independent electrostatic measurement of the separation distance was taken [2,26–30]. The measured asymmetric lateral Casimir force was observed from its nonsinusoidal phase dependence, as shown in Figure 4a. Here, the measurement data are compared with the exact theory describing the Rayleigh scattering [31] of the electromagnetic oscillations on the sinusoidally corrugated boundary surfaces of a sphere and plate with no fitting parameters. In Figure 4a, both the experimental data shown as dots and the theoretical line shown in red demonstrate that the lateral Casimir force is asymmetric and that the dependence of the lateral Casimir force as function of the phase is purely sinusoidal only if the calculation is restricted to the lowest order in the corrugation amplitudes. The asymmetry of the lateral Casimir force can be clearly observed even without the red theoretical curve, because the average shift of the maxima from the midpoint of two adjacent minima is $(0.12 \pm 0.02)\lambda$. The experimental data of the measured lateral Casimir force amplitude as a function of separation are shown in Figure 4b as crosses, along with error bars. These data were found to be in good agreement with the theory, which takes into account the photon correlation. In Figure 4b, the measured forces are found to deviate from the PFA, which neglects diffraction effects. This experiment using large amplitude corrugations with a significatly smaller period allowed demonstration of the asymmetry of the lateral Casimir force and had the ability to quantify deviations from the PFA.

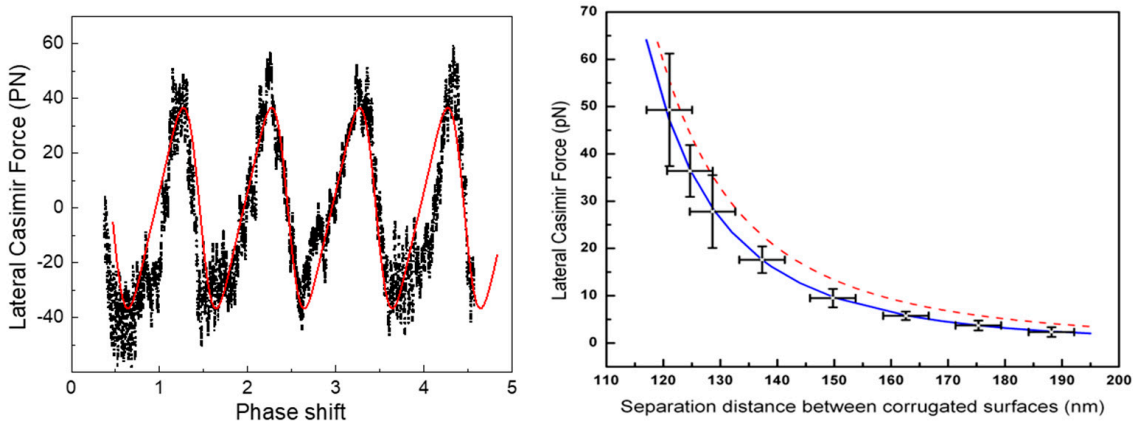

(**a**) (**b**)

Figure 4. (**a**) The measured lateral Casimir force for a separation distance of $z = 124.7 \pm 4.0$ nm as a function of the phase shift between the corrugations (black dots) compared with the theory (red solid line) given by the Rayleigh scattering approach [29]. Note that the maximum is not at the midpoint of the minima, demonstrating asymmetry. (**b**) The amplitude as a function of separation distance (shown with error bars) compared to the Rayleigh scattering theory, which includes photon correlation (blue solid line), and to the PFA with no photon correlation (red dashed line) [30].

3.2. Role of Coherent Scattering in the Normal Casimir Force between Two Uniformly Corrugated Surfaces

Whereas the lateral Casimir force acts parallel to the two corrugated surfaces, the normal Casimir force is measured perpendicular to the periodically corrugated surfaces and provides us with valuable insight into the macroscopic geometric effects of vacuum fluctuations. As in Section 3.1, these geometry effects are quantified in terms of deviation from PFA where the Casimir energy is treated as the simple addition of flat infinitesimal surface elements which represent the curved surface. In addition to neglecting diffraction effects, the PFA ignores correlations from the interplay of geometry, material properties, and temperature.

The measurement of the normal Casimir force between two sinusoidally corrugated diffraction gratings on a gold-coated plate and sphere at various angles between corrugations was previously reported in Refs. [32,41]. The data are shown in Figure 5a where the measured Casimir force is shown to increase by 15% at 130 nm separation when the orientation angle between corrugations increased from 0 to 2.4. Figure 5b shows the deviation of the measured force from PFA for an angle between the corrugations of 1.2°. The measured forces are seen to deviate from the PFA (deviations measure diffraction-like coherent effects not included in PFA) and to be in agreement with the gradient approximation theory [42,43] including correlation effects of geometry and real metal–dielectric properties. The system is also seen to be highly sensitive to the role of thermal photons and is thus a measurement of the thermal Casimir effect between corrugated surfaces.

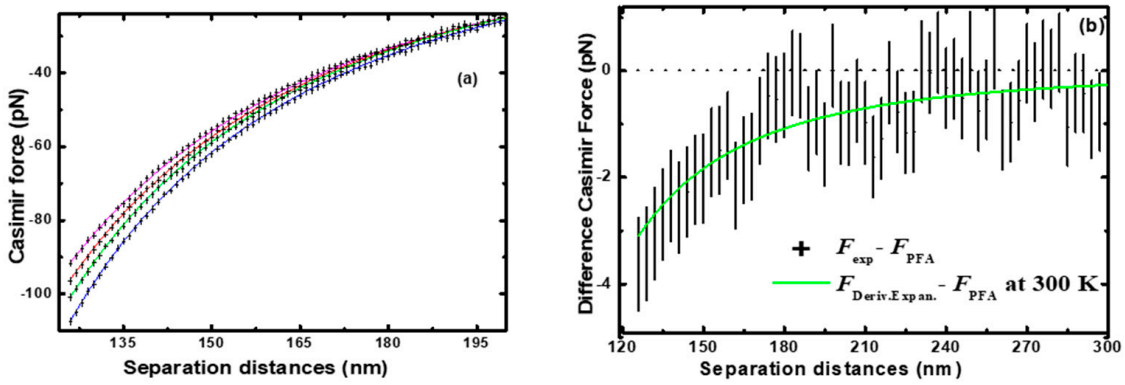

Figure 5. (**a**) Measured (shown with error bars) normal Casimir force between two sinusoidally corrugated surfaces corresponding to corrugation orientation angles of 0°, 1.2°, 1.8°, and 2.4° (top to bottom) compared to the theory (solid lines) using the derivative expansion [32]. (**b**) The difference ($F_{exp} - F_{PFA}$) between the measured and PFA-predicted Casimir forces (shown with error bars) for a corrugation orientation angle of 1.2° compared to the corresponding difference ($F_{Deriv\ Expan} - F_{PFA}$) between the gradient expansion and PFA theories at T = 300 K [41]. This difference a measure of the correlation and diffraction effects (see text for details). The bars represent the total (combined systematic and random) errors at a 67% confidence level.

The above results experimentally demonstrate the angle dependence of the normal Casmir force between a corrugated plate and corrugated sphere. The strong angular and temperature dependences of normal Casimir force for two oriented corrugations make it a uniquely important system for understanding the nontrivial combined interactions of geometry, material properties, and temperature.

4. Role of Magnetic Fluctuations in the Casimir Force

More than 40 years after the prediction of potentially repulsive contributions from magnetic fluctuations [44,45], the first experimental demonstration of the role of magnetic permeability, μ, was reported [14,15] and the results were compared to a new measurement with non-magnetic Au surfaces [6]. The use of materials such as Ni with $\mu > 0$ reduces

the Casimir force by adding a repulsive contribution. The experiments also showed that the role of electrostatic patch charges on surfaces was negligible in our experimental scheme. In Ref. [14], we reported the first demonstration of the Casimir force between two ferromagnetic Ni boundary surfaces. The experimental data, as shown in Figure 6, were found to be in good agreement with the predictions of the Lifshitz theory for magnetic boundary surfaces combined with the dissipation-less plasma model approach to describe the low-frequency permittivity of the metal. Tabulated [11] values of ε and μ were used, except for the dissipation $\gamma = 0$ (plasma) or $\gamma > 0$ (Drude model) for the low-frequency response of Au.

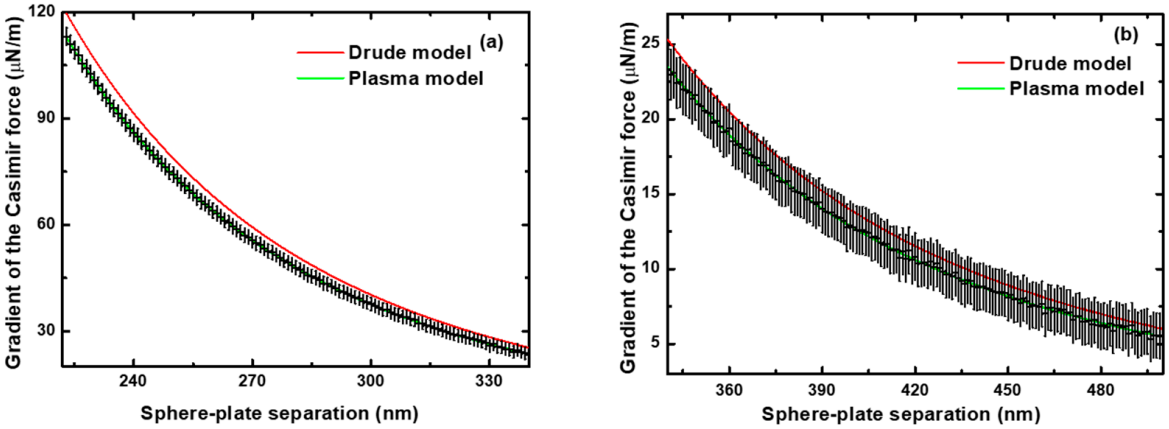

Figure 6. Measured (shown with error bars) Casimir force gradient between a ferromagnetic Ni-coated sphere and plate at small (**a**) and large (**b**) separation distances [14]. The bars represent total error at a 67% confidence level. The experimental data are in remarkable agreement with the plasma model with magnetic properties of Ni included. There are no fitting parameters used.

In Ref. [15], the measured gradient of the Casimir force between a Ni plate and the non-magnetic Au sphere was reported. The mean gradient of the Casimir force (see Figure 7) was compared with theoretical predictions of the Lifshitz theory with no fitting parameters. The data are in good greement with both the plasma model and Drude model description of the metal-free electrons as they coincide for these separations.

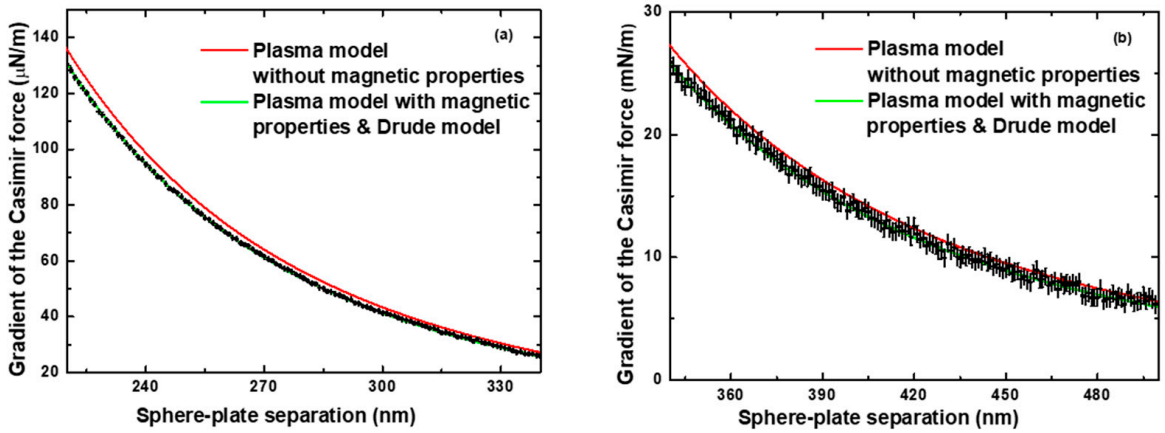

Figure 7. Measured (shown with error bars) Casimir force between an Au sphere–ferromagnetic Ni plate versus small (**a**) and large (**b**) surface separation distances [15]. The error bars represent total error bars at a 67% confidence level. The experimental data are in good agreement with both the plasma model ($\gamma = 0$) and the Drude model for low-frequency metal response with the tabulated ε and μ of Ni included. The Drude and plasma models overlap for the μ of Ni in this region. No fitting parameters were used in comparison.

Conclusion on Role of Electrostatic Patches

To answer the critical question of whether zero-point photons dissipate energy on free electron scattering, one has to show agreement with either the plasma (no dissipation) or Drude (dissipative) model. For the Au-coated sphere and plate, using a different tabulated ε and μ to calculate the theoretical Casimir force makes a negligible difference [14,15] to the agreement with the dissipationless plasma model. However, for non-magnetic materials, an agreement can possibly be brought about by using electrostatic forces [21,23] with specialized charge density and size distributions. Yet, from the results of the experiments indicated in Figures 3, 6 and 7, one can see that anomalous forces from electrostatic patches in the experiments (a) have to be negligible and (b) cannot explain the difference from the Drude model consistently. To bring about an agreement with Drude model, one needs positive contribution in Figure 6 (two magnetic material surfaces), but a negative one in Figure 3 (non-magnetic material surfaces). In the experiment in Figure 7 with one magnetic material and one non-magnetic material, both models overlap and agree with data for this separation region. As electric patch forces only add to the total force, the only consistent explanation is that they have to be negligible [46,47]. Following these results, a difference force measurement [16] showed that the non-dissipative plasma model was in remarkable agreement and the dissipative Drude model in disagreement with their data by a factor of 10^3.

5. Precision Casimir Force Measurements with Graphene

Unlike normal metals, where for comparison between experiment and theory, the metal properties have to be input from tabulated values with extrapolation to zero frequency, the non-local response function of graphene to electromagnetic fluctuations can be calculated from the first principles of quantum electrodynamics [48–50]. Another interesting feature is an unusually large thermal correction to the Casimir force between two parallel graphene sheets spaced at separations of less than 1 μm, first predicted by Gómez-Santos [51]. Many physical effects in graphene have also been described [52]. In a more recent measurement [53], the gradient of the Casimir force between an Au-coated microsphere and a graphene sheet deposited on a silica glass (SiO_2) plate obtained in a high vacuum using a custom dynamic AFM was performed. In the previous experiment [53], the graphene sheet was deposited on a SiO_2 film covering a Si plate. The gradient of the Casimir force was measured and found to be in good agreement with the theory. However, the thermal effect could not be identified because of the large uncertainty in the charge carrier concentration of the Si plate used.

In this Casimir force gradient measurement system, a tipless AFM cantilever was used whose spring constant was reduced through chemical etching, as described above. As in previous experiments, a hollow glass microsphere attached to the end of the cantilever using silver epoxy and coated with Au was used as the second surface. The thickness of the Au coating and the diameter of the coated sphere were measured to be 120.3 nm and 120.7 μm, using an AFM and a scanning electron microscope, respectively. The rms roughness of the Au coating was measured to be δ = 0.9 nm. The resonant frequency of the complete Au-coated cantilever–sphere system in the vacuum was measured to be $\omega_0 = 6.1581 \times 10^3$ rad/s.

A large area of graphene monolayer originally grown by chemical vapor deposition on a Cu foil was transferred onto a polished JGS2 grade fused silica double-sided optically polished substrate of 100 mm diameter and 500 μm thickness through an electro-chemical delamination procedure. A 1×1 cm^2 piece of the graphene-coated fused silica wafer was then cut from the large sample and used. After the force gradient measurements, the roughness of the graphene on the fused silica substrate was measured to be $\delta = 1.5 \pm 0.1$ nm using an AFM. After the Casimir force gradient measurement, the impurity concentration of graphene was determined utilizing Raman spectroscopy. The respective zero-temperature value of the chemical potential for our sample is given by $\mu = 0.24 \pm 0.01$ eV. The values of the energy gap Δ for graphene on a SiO_2 substrate vary between 0.01 eV and 0.2 eV.

The fused silica-supported graphene sample and gold sphere probe were loaded into the vacuum chamber which was pumped down to a pressure below 9×10^{-9} Torr. Because of the sensitive nature of the graphene sample, the UV/Ar-ion radiation treatment described in Section 2 for cleaning the Au surfaces was not implemented, to avoid potential damage to the single atomic layer of graphene. To ensure the accuracy of the measurement, the residual potential difference between the gold and graphene surfaces was determined through the same standard electrostatic calibration procedure as stated in Section 2. The change in the resonant frequency Δf in the presence of external force was recorded by the PLL (phase-locked loop) every 0.14 nm while the graphene plate was moved toward the grounded sphere, starting at the maximum separation. This was repeated with one of ten different voltages V_i that varied between 0.083 V and 0.183 V and eleven voltages equal to the residual potential difference V_0 (see below) applied to the graphene using ohmic contacts while the sphere remained grounded.

The gradients of the total and Casimir forces were calculated from the measured frequency shifts using electrostatic calibration. At each separation, the gradient of the Casimir force was measured 21 times with the different applied voltages mentioned above. The random errors of the mean were determined at a 67% confidence level and combined in quadrature with the systematic errors originating primarily from the errors in measuring the frequency shifts. The obtained measurement data for the force gradient with their errors are shown in Figure 8 as crosses corresponding to error bars. For visual clarity, in Figure 8a, all data points are indicated, whereas in Figure 8b,c, every other data point and in Figure 8d, only every third are shown. For the comparison with the theory, the relativistic version of the Lifshitz formula with reflection coefficients expressed via the exact polarization tensor of graphene in the framework of the Dirac model takes into account the nonzero energy gap, Δ. and chemical potential, μ [54–57]. The computational results for the boundaries of allowed theoretical bands are shown in Figure 8 by the two bands, computed at T = 294 K and T = 0 K. The upper line in each band was computed for μ = 0.25 eV, Δ = 0 eV, and the lower line for μ = 0.23 eV, Δ = 0.2 eV. As shown in Figure 8, the measurement data are in very good agreement with the theory at T = 294 K. The unusually large thermal effect in the force gradient equal to the difference between the top and bottom bands is clearly demonstrated over the region from 250 to 590 nm. For example, at sphere–plate separations of 250, 300, 400, 500, and 590 nm, the thermal corrections were 4%, 5%, 7%, 8.5%, and 10% of the total force gradient, respectively.

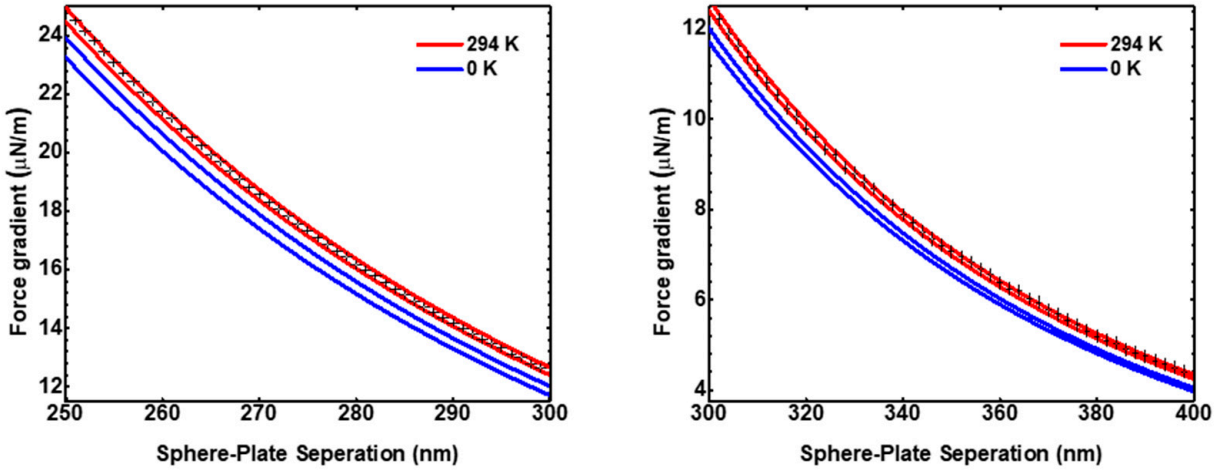

Figure 8. *Cont.*

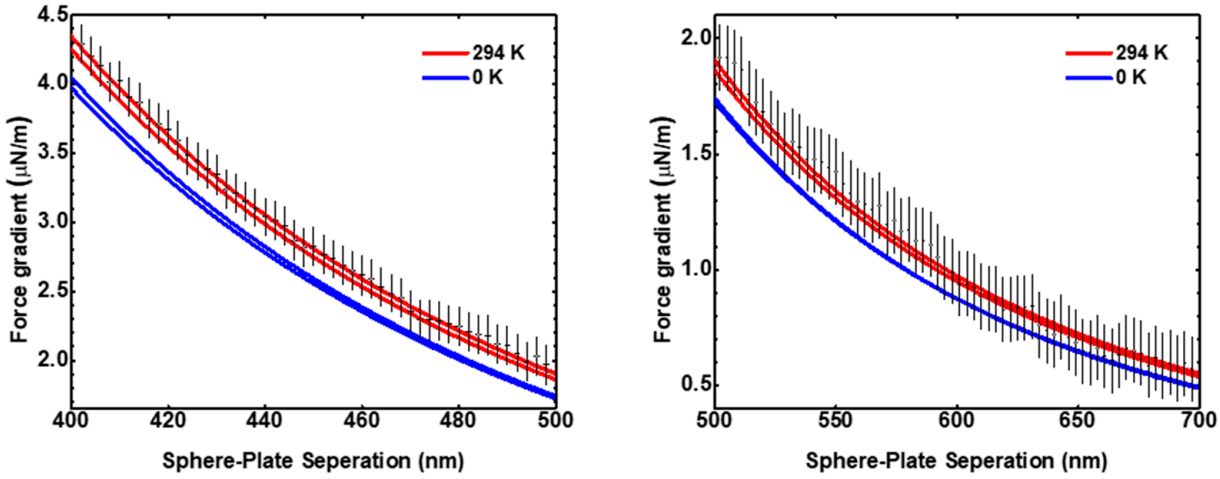

(**c**) (**d**)

Figure 8. The measured (shown with error bars) mean gradient of the Casimir force as a function of separation compared to the calculations at T = 294 K (red) and 0 K (blue) with the upper lines for each T band computed for the chemical potential μ = 0.25 eV and the gap Δ = 0 eV, and the lower lines for μ = 0.23 eV, Δ = 0.2 eV [58,59]. The agreement of the data with the T = 294 K band is the detection of the thermal Casimir effect with graphene at sphere–plate separations of 250–300 nm (**a**), 300–400 nm (**b**), 400–500 nm (**c**), and 500–700 nm (**d**).

6. Conclusions

Precision Casimir force measurements have undergone remarkable progress over the last two decades. Some of the results of the UC Riverside group are presented above. The experimental results have, in turn, encouraged a tremendous amount of theoretical developments, some detailed in Ref. [60]. In addition to improvements in experimental methodology, considerable rogress has also been achieved with the use of complicated geometries [61,62] other than the sinusoidally corrugated cases discussed above. Many other exciting geometric dependences [63–66] and material-dependent repulsive forces [9,67–71] remain to be investigated and exploited in nanomechanical devices [72,73]. Casimir torques [74,75] and their experimental exploitation represent another area of much promise. An exciting and as yet unresolved issue that remains is the disagreement between the experiment and the Lifshitz theory [76–79] when the dielectric response of metals is deduced from the optical data extrapolated down to zero frequency by means of the Drude model, where the relaxation parameter γ describes the energy losses of conduction electrons due to phonon scattering. It has been a puzzle that agreement between experiment and theory is obtained only if one makes γ equal to zero. This might lead to the conclusion that are no energy losses at low frequencies for zero-point photon interactions with materials, unlike the case of real photons. However, this hypothesis alone would lead to the violation of the fluctuation dissipation theorem which is central to all of physics. Much light was shed from the precision experiments with graphene, discussed above, where the dielectric response of graphene was calculated from first principles of quantum electrodynamics. Based on the graphene's dielectric response, it appears that it is the phenomenological character of the Drude model at low frequencies that might be in error. In particular, the Drude model does not capture the complete wave vector dependence of the dielectric response for evanescent waves, which are electromagnetic fluctuations that are not on the mass shell. Here again, there have been suggestions [80] for how to bring about a resolution to this long-standing problem, which are discussed elsewhere in Ref. [60].

Author Contributions: Both authors contributed equally to this work. All authors have read and agreed to the published version of the manuscript.

Funding: The work of M.D. and U.M. was partially supported by the National Science Foundation Grant No. PHY-2012201.

Data Availability Statement: The data are from the references cited.

Conflicts of Interest: The authors declare no conflict of interest.

References

1. Mohideen, U.; Roy, A. Precision measurement of the Casimir force from 0.1 to 0.9 mm. *Phys. Rev. Lett.* **1998**, *81*, 4549–4552. [CrossRef]
2. Chen, F.; Mohideen, U.; Klimchitskaya, G.L.; Mostepanenko, V.M. Experimental and theoretical investigation of the lateral Casimir force between corrugated surfaces. *Phys. Rev. A* **2002**, *66*, 032113. [CrossRef]
3. Harris, B.W.; Chen, F.; Mohideen, U. Precision measurement of the Casimir force using gold surfaces. *Phys. Rev. A* **2000**, *62*, 052109. [CrossRef]
4. Decca, R.S.; Lopez, D.; Fischbach, E.; Klimchitskaya, G.L.; Krause, D.E.; Mostepanenko, V.M. Precise comparison of theory and new experiment for the Casimir force leads to stronger constraints on thermal quantum effects and long-range interactions. *Ann. Phys.* **2005**, *318*, 37–80. [CrossRef]
5. Decca, R.S.; Lopez, D.; Fischbach, E.; Klimchitskaya, G.L.; Krause, D.E.; Mostepanenko, V.M. Tests of new physics from precise measurements of the Casimir pressure between two gold-coated plates. *Phys. Rev. D* **2007**, *75*, 077101. [CrossRef]
6. Chang, C.-C.; Banishev, A.A.; Castillo-Garza, R.; Klimchitskaya, G.L.; Mostepanenko, V.M.; Mohideen, U. Gradient of the Casimir force between Au surfaces of a sphere and a plate measured using an atomic force microscope in a frequency-shift technique. *Phys. Rev. B* **2012**, *85*, 165443. [CrossRef]
7. Bordag, M.; Klimchitskaya, G.L.; Mohideen, U.; Mostepanenko, V.M. *Advances in the Casimir Effect*; Oxford University Press: Oxford, UK, 2015. [CrossRef]
8. Klimchitskaya, G.L.; Mohideen, U.; Mostepanenko, V.M. The Casimir force between real materials: Experiment and theory. *Rev. Mod. Phys.* **2009**, *81*, 1827–1885. [CrossRef]
9. Woods, L.M.; Dalvit, D.A.R.; Tkatchenko, A.; Rodriguez-Lopez, P.; Rodriguez, A.W.; Podgornik, R. Materials perspective on Casimir and van der Waals interactions. *Rev. Mod. Phys.* **2016**, *88*, 045003. [CrossRef]
10. Bordag, M.; Mohideen, U.; Mostepanenko, V. New developments in the Casimir effect. *Phys. Rep.* **2001**, *353*, 1–205. [CrossRef]
11. Palik, E.D. (Ed.) *Handbook of Optical Constants of Solids*; Academic Press: San Diego, CA, USA, 1985. [CrossRef]
12. Garcia-Sanchez, D.; Fong, K.Y.; Bhaskaran, H.; Lamoreaux, S.; Tang, H.X. Casimir force and in situ surface potential measurements on nanomembranes. *Phys. Rev. Lett.* **2012**, *109*, 027202. [CrossRef]
13. Sushkov, A.O.; Kim, W.J.; Dalvit, D.A.R.; Lamoreaux, S.K. Observation of the thermal Casimir force. *Nat. Phys.* **2011**, *7*, 230–233. [CrossRef]
14. Banishev, A.; Klimchitskaya, G.; Mostepanenko, V.; Mohideen, U. Demonstration of the Casimir force between ferromagnetic surfaces of a Ni-coated sphere and a Ni-coated plate. *Phys. Rev. Lett.* **2013**, *110*, 137401. [CrossRef] [PubMed]
15. Banishev, A.A.; Chang, C.-C.; Klimchitskaya, G.L.; Mostepanenko, V.M.; Mohideen, U. Measurement of the gradient of the Casimir force between a nonmagnetic gold sphere and a magnetic nickel plate. *Phys. Rev. B* **2012**, *85*, 195422. [CrossRef]
16. Bimonte, G.; Lopez, D.; Decca, R.S. Isoelectronic determination of the thermal Casimir force. *Phys. Rev. B* **2016**, *93*, 184434. [CrossRef]
17. Xu, J.; Klimchitskaya, G.L.; Mostepanenko, V.M.; Mohideen, U. Reducing detrimental electrostatic effects in Casimir-force measurements and Casimir-force-based microdevices. *Phys. Rev. A* **2018**, *97*, 032501. [CrossRef]
18. Liu, M.Y.; Xu, J.; Klimchitskaya, G.L.; Mostepanenko, V.M.; Mohideen, U. Precision measurement of the gradient of the Casimir force between ultraclean metallic surfaces at larger separations. *Phys. Rev. A* **2019**, *100*, 052511. [CrossRef]
19. Liu, M.Y.; Xu, J.; Klimchitskaya, G.L.; Mostepanenko, V.M.; Mohideen, U. Examining the Casimir puzzle with an upgraded AFM-based technique and advanced surface cleaning. *Phys. Rev. B* **2019**, *100*, 081406. [CrossRef]
20. Liu, M.Y.; Schafer, R.; Xu, J.; Mohideen, U. Elimination of electrostatic forces in precision Casimir force measurements using UV and Ar ion radiation. *Mod. Phys. Lett. A* **2020**, *35*, 2040001. [CrossRef]
21. Behunin, R.; Intravaia, F.; Dalvit, D.; Neto, P.M.; Reynaud, S. Modeling electrostatic patch effects in Casimir force measurements. *Phys. Rev. A* **2012**, *85*, 012504. [CrossRef]
22. Behunin, R.O.; Dalvit, D.A.R.; Decca, R.S.; Genet, C.; Jung, I.W.; Lambrecht, A.; Liscio, A.; Lopez, D.; Reynaud, S.; Schnoering, G.; et al. Kelvin probe force microscopy of metallic surfaces used in Casimir force measurements. *Phys. Rev. A* **2014**, *90*, 062115. [CrossRef]
23. Behunin, R.O.; Zeng, Y.; Dalvit, D.A.R.; Reynaud, S. Electrostatic patch effects in Casimir-force experiments performed in the sphere-plane geometry. *Phys. Rev. A* **2012**, *86*, 052509. [CrossRef]
24. Naji, A.; Dean, D.S.; Sarabadani, J.; Horgan, R.R.; Podgornik, R. Fluctuation-induced interaction between randomly charged dielectrics. *Phys. Rev. Lett.* **2010**, *104*, 060601. [CrossRef] [PubMed]

25. Roy, A.; Mohideen, U. Demonstration of the nontrivial boundary dependence of the Casimir force. *Phys. Rev. Lett.* **1999**, *82*, 4380–4383. [CrossRef]
26. Chen, F.; Mohideen, U.; Klimchitskaya, G.L.; Mostepanenko, V.M. Demonstration of the lateral Casimir force. *Phys. Rev. Lett.* **2002**, *88*, 101801. [CrossRef] [PubMed]
27. Derjaguin, B. Untersuchungen über die Reibung und Adhäsion, IV. Theorie des Anhaftens kleiner Teilcher. *Kolloid-Zeitschrift* **1934**, *69*, 155–164. [CrossRef]
28. Blocki, J.; Randrup, J.; Swiatecki, W.J.; Tsang, C.F. Proximity forces. *Ann. Phys.* **1977**, *105*, 427–462. [CrossRef]
29. Chiu, H.C.; Klimchitskaya, G.L.; Marachevsky, V.N.; Mostepanenko, V.M.; Mohideen, U. Demonstration of the asymmetric lateral Casimir force between corrugated surfaces in the nonadditive regime. *Phys. Rev. B* **2009**, *80*, 121402. [CrossRef]
30. Chiu, H.C.; Klimchitskaya, G.L.; Marachevsky, V.N.; Mostepanenko, V.M.; Mohideen, U. Lateral Casimir force between sinusoidally corrugated surfaces: Asymmetric profiles, deviations from the proximity force approximation, and comparison with exact theory. *Phys. Rev. B* **2010**, *81*, 115417. [CrossRef]
31. Lord Rayleigh, Strutt, J.W. On the dynamical theory of gratings. *Proc. R. Soc. Lond. A* **1907**, *79*, 399–416. [CrossRef]
32. Banishev, A.; Wagner, J.; Emig, T.; Zandi, R.; Mohideen, U. Demonstration of angle-dependent Casimir force between corrugations. *Phys. Rev. Lett.* **2013**, *110*, 250403. [CrossRef]
33. Chan, H.B.; Bao, Y.; Zou, J.; Cirelli, R.; Klemens, F.; Mansfield, W.; Pai, C. Measurement of the Casimir force between a gold sphere and a silicon surface with nanoscale trench array. *Phys. Rev. Lett.* **2008**, *101*, 030401. [CrossRef] [PubMed]
34. Bao, Y.; Gue'rout, R.; Lussange, J.; Lambrecht, A.; Cirelli, R.A.; Klemens, F.; Mansfield, W.M.; Pai, C.S.; Chan, H.B. Casimir force on a surface with shallow nanoscale corrugations: Geometry and finite conductivity effects. *Phys. Rev. Lett.* **2010**, *105*, 250402. [CrossRef]
35. Golestanian, R.; Kardar, M. Mechanical Response of Vacuum. *Phys. Rev. Lett.* **1997**, *78*, 3421–3425. [CrossRef]
36. Rodrigues, R.B.; Neto, P.A.M.; Lambrecht, A.; Reynaud, S. Lateral Casimir force beyond the proximity-force approximation. *Phys. Rev. Lett.* **2006**, *96*, 100402. [CrossRef]
37. Canaguier-Durand, A.; Neto, P.A.M.; Lambrecht, A.; Reynaud, S. Thermal Casimir effect for Drude metals in the plane-sphere geometry. *Phys. Rev. A* **2010**, *82*, 012511. [CrossRef]
38. Zandi, R.; Emig, T.; Mohideen, U. Quantum and thermal Casimir interaction between a sphere and a plate: Comparison of Drude and plasma models. *Phys. Rev. B* **2010**, *81*, 195423. [CrossRef]
39. Rosa, F.S.S.; Dalvit, D.A.R.; Milonni, P.W. Casimir-Lifshitz theory and metamaterials. *Phys. Rev. Lett.* **2008**, *100*, 183602. [CrossRef] [PubMed]
40. Rodrigues, R.B.; Neto, P.A.M.; Lambrecht, A.; Reynaud, S. Vacuum-induced torque between corrugated metallic plates. *Europhys. Lett.* **2006**, *76*, 822. [CrossRef]
41. Banishev, A.A.; Wagner, J.; Emig, T.; Zandi, R.; Mohideen, U. Experimental and theoretical investigation of the angular dependence of the Casimir force between sinusoidally corrugated surfaces. *Phys. Rev. B* **2014**, *89*, 235436. [CrossRef]
42. Bimonte, G.; Emig, T.; Jaffe, R.L.; Kardar, M. Casimir forces beyond the proximity approximation. *Europhys. Lett.* **2012**, *97*, 50001. [CrossRef]
43. Bimonte, G.; Emig, T.; Kardar, M. Material dependence of Casimir forces: Gradient expansion beyond proximity. *Appl. Phys. Lett.* **2012**, *100*, 074110. [CrossRef]
44. Barash, Y.S.; Ginzburg, V.L. Electromagnetic fluctuations in matter and molecular (Van-der-Waals) forces between them. *Sov. Phys. Usp.* **1975**, *18*, 305–322. [CrossRef]
45. Kenneth, O.; Klich, I.; Mann, A.; Revzen, M. Repulsive Casimir forces. *Phys. Rev. Lett.* **2002**, *89*, 033001. [CrossRef] [PubMed]
46. Bezerra, V.B.; Klimchitskaya, G.L.; Mohideen, U.; Mostepanenko, V.M.; Romero, C. Impact of surface imperfections on the Casimir force for lenses of centimeter-size curvature radii. *Phys. Rev. B* **2011**, *83*, 075417. [CrossRef]
47. Decca, R.S.; Fischbach, E.; Klimchitskaya, G.L.; Krause, D.E.; Lopez, D.; Mohideen, U.; Mostepanenko, V.M. Capacitance measurements and electrostatic calibrations in experiments measuring the Casimir force. *Int. J. Mod. Phys. A* **2011**, *26*, 3930–3943. [CrossRef]
48. Drosdoff, D.; Woods, L.M. Quantum and thermal dispersion forces: Application to graphene nanoribbons. *Phys. Rev. Lett.* **2014**, *112*, 025501. [CrossRef]
49. Rodriguez-Lopez, P.; Kort-Kamp, W.J.M.; Dalvit, D.A.R.; Woods, L.M. Casimir force phase transitions in the graphene family. *Nat. Commun.* **2017**, *8*, 14699. [CrossRef]
50. Klimchitskaya, G.L.; Mohideen, U.; Mostepanenko, V.M. Theory of the Casimir interaction from graphene-coated substrates using the polarization tensor and comparison with experiment. *Phys. Rev. B* **2014**, *89*, 115419. [CrossRef]
51. Gomez-Santos, G. Thermal van der Waals interaction between graphene layers. *Phys. Rev. B* **2009**, *80*, 245424. [CrossRef]
52. Sarabadani, J.; Naji, A.; Asgari, R.; Podgornik, R. Many-body effects in the van der Waals–Casimir interaction between grphene layers. *Phys. Rev. B* **2011**, *84*, 155407. [CrossRef]
53. Banishev, A.A.; Wen, H.; Xu, J.; Kawakami, R.K.; Klimchitskaya, G.L.; Mostepanenko, V.M.; Mohideen, U. Measuring the Casimir force gradient from graphene on a SiO_2 substrate. *Phys. Rev. B* **2013**, *87*, 205433. [CrossRef]
54. Bordag, M.; Klimchitskaya, L.; Mostepanenko, M.; Petrov, M. Quantum field theoretical description for the reflectivity of graphene. *Phys. Rev. D* **2016**, *93*, 089907. [CrossRef]

55. Bimonte, G.; Klimchitskaya, G.L.; Mostepanenko, V.M. Thermal effect in the Casimir force for graphene and graphene-coated substrates: Impact of nonzero mass gap and chemical potential. *Phys. Rev. B* **2017**, *96*, 115430. [CrossRef]
56. Sernelius, B.E. Retarded interactions in graphene systems. *Phys. Rev. B* **2014**, *89*, 079901. [CrossRef]
57. Klimchitskaya, G.L.; Mostepanenko, V.M.; Sernelius, B.E. Two approaches for describing the Casimir interaction in graphene: Density-density correlation function versus polarization tensor. *Phys. Rev. B* **2014**, *89*, 125407. [CrossRef]
58. Liu, M.; Zhang, Y.; Klimchitskaya, G.L.; Mostepanenko, V.M.; Mohideen, U. Demonstration of an unusual thermal effect in the casimir force from graphene. *Phys. Rev. Lett.* **2021**, *126*, 206802. [CrossRef] [PubMed]
59. Liu, M.; Zhang, Y.; Klimchitskaya, G.L.; Mostepanenko, V.M.; Mohideen, U. Experimental and theoretical investigation of the thermal effect in the Casimir interaction from graphene. *Phys. Rev. B* **2021**, *104*, 085436. [CrossRef]
60. Klimchitskaya, G.L.; Mostepanenko, V.M. (Eds.) *Special Issue: 75 Years of the Casimir Effect: Advances and Prospects*; *Physics*, *in print*. Available online: https://www.mdpi.com/journal/physics/special_issues/75yearsCasimir (accessed on 17 March 2024).
61. Intravaia, F.; Koev, S.; Jung, I.W.; Talin, A.A.; Davids, P.S.; Decca, R.S.; Aksyuk, V.A.; Dalvit, D.A.R.; López, D. Strong Casimir force reduction through metallic surface nanostructuring. *Nat. Commun.* **2013**, *4*, 2515. [CrossRef]
62. Tang, L.; Wang, M.; Ng, C.Y.; Nikolic, M.; Chan, C.T.; Rodriguez, A.W.; Chan, H.B. Measurement of non-monotonic Casimir forces between silicon nanostructures. *Nat. Photon.* **2017**, *11*, 97–101. [CrossRef]
63. Rahi, S.J.; Emig, T.; Graham, N.; Jaffe, R.L.; Kardar, M. Scattering theory approach to electrodynamic Casimir forces. *Phys. Rev. D* **2009**, *80*, 085021. [CrossRef]
64. Lambrecht, A.; Neto, P.A.; Reynaud, S. The Casimir effect within scattering theory. *New J. Phys.* **2006**, *8*, 243. [CrossRef]
65. Maghrebi, M.F.; Rahi, S.J.; Emig, T.; Graham, N.; Jaffe, R.L.; Kardara, M. Analytical results on Casimir forces for conductors with edges and tips. *Proc. Natl. Acad. Sci. USA* **2011**, *108*, 6867–6871. [CrossRef]
66. Milton, K.A.; Wagner, J. Multiple scattering methods in Casimir calculations. *J. Phys. A Math. Theor.* **2008**, *41*, 155402. [CrossRef]
67. Grushin, A.G.; Cortijo, A. Tunable Casimir repulsion with three-dimensional topological insulators. *Phys. Rev. Lett.* **2011**, *106*, 020403. [CrossRef]
68. Jiang, Q.; Wilczek, F. Chiral Casimir forces: Repulsive, enhanced, tunable. *Phys. Rev. B* **2019**, *99*, 125403. [CrossRef]
69. Somers, D.A.; Munday, J.N. Conditions for repulsive Casimir forces between identical birefringent materials. *Phys. Rev. A* **2017**, *95*, 022509. [CrossRef]
70. Tajik, F.; Palasantzas, G. Sensitivity of actuation dynamics of Casimir oscillators on finite temperature with topological insulator materials: Response of repulsive vs attractive interactions. *Phys. Lett. A* **2023**, *481*, 129032. [CrossRef]
71. Gelbwaser-Klimovsky, D.; Graham, N.; Kardar, M.; Krüger, M. Equilibrium forces on nonreciprocal materials. *Phys. Rev. B* **2022**, *106*, 115106. [CrossRef]
72. Rodriguez, A.W.; Capasso, F.; Johnson, S.G. The Casimir effect in microstructured geometries. *Nat. Photon.* **2011**, *5*, 211–221. [CrossRef]
73. Javor, J.; Yao, Z.; Imboden, M.; Campbell, D.K.; Bishop, D.J. Analysis of a Casimir-driven parametric amplifier with resilience to Casimir pull-in for MEMS single-point magnetic gradiometry. *Microsyst. Nanoeng.* **2021**, *7*, 73. [CrossRef] [PubMed]
74. Munday, J.N.; Iannuzzi, D.; Barash, Y.; Capasso, F. Torque on birefringent plates induced by quantum fluctuations. *Phys. Rev. A* **2005**, *71*, 042102. [CrossRef]
75. Broer, W.; Lu, B.; Podgornik, R. Qualitative chirality effects on the Casimir-Lifshitz torque with liquid crystals. *Phys. Rev. Res.* **2021**, *3*, 033238. [CrossRef]
76. Boström, M.; Sernelius, B.E. Thermal effects on the Casimir force in the 0.1–5 μm range. *Phys. Rev. Lett.* **2000**, *84*, 4757–4760. [CrossRef] [PubMed]
77. Genet, C.; Lambrecht, A.; Reynaud, S. Temperature dependence of the Casimir effect between metallic mirrors. *Phys. Rev. A* **2000**, *62*, 012110. [CrossRef]
78. Bordag, M.; Geyer, B.; Klimchitskaya, G.L.; Mostepanenko, V.M. Casimir force at both nonzero temperature and finite conductivity. *Phys. Rev. Lett.* **2000**, *85*, 503–506. [CrossRef] [PubMed]
79. Milton, K.A. The Casimir effect: Recent controversies and progress. *J. Phys. A Math. Gen.* **2004**, *37*, R209–R277. [CrossRef]
80. Klimchitskaya, G.L.; Mostepanenko, V.M.; Svetovoy, V.B. Probing the response of metals to low-frequency s-polarized evanescent fields. *EPL (Europhys. Lett.)* **2022**, *139*, 66001. [CrossRef]